

Article

The Effect of Cutting Tool Geometry on Surface Integrity: A Case Study of CBN Tools and the Inner Surface of Bearing Rings

Lenka Cepova ¹, Robert Cep ¹, Leszek Chalko ², Stepanka Dvorackova ³, Miroslav Trochta ¹,
Miroslaw Rucki ^{2,*}, Libor Beranek ⁴, Ondrej Mizera ¹ and Volodymyr Chyshkala ⁵

¹ Faculty of Mechanical Engineering, VSB-Technical University of Ostrava, 17. Listopadu 2172/15, 708 00 Ostrava, Czech Republic

² Faculty of Mechanical Engineering, Kazimierz Pulaski University of Technology and Humanities in Radom, Stasieckiego 54, 26-600 Radom, Poland

³ Faculty of Mechanical Engineering, Technical University of Liberec, Studentska 2, 461 17 Liberec, Czech Republic

⁴ Faculty of Mechanical Engineering, Czech Technical University of Prague, Technicka 4, 166 07 Prague, Czech Republic

⁵ Department of Reactor Engineering Materials and Physical Technologies, V. N. Karazin Kharkiv National University, 4 Svobody Sq., 61022 Kharkiv, Ukraine

* Correspondence: m.rucki@uthrad.pl

Featured Application: Specifically, this application deals with cubic boron nitride (CBN) cutting tool selection for the machining of steel 100Cr6 thin-walled bearing rings, but the methodology and findings can be extended to other sorts of turning.



Citation: Cepova, L.; Cep, R.; Chalko, L.; Dvorackova, S.; Trochta, M.; Rucki, M.; Beranek, L.; Mizera, O.; Chyshkala, V. The Effect of Cutting Tool Geometry on Surface Integrity: A Case Study of CBN Tools and the Inner Surface of Bearing Rings. *Appl. Sci.* **2023**, *13*, 3543. <https://doi.org/10.3390/app13063543>

Academic Editors: Michael Oluwatosin Bodunrin, Desmond Klenam and Japheth Obiko

Received: 17 January 2023

Revised: 4 March 2023

Accepted: 8 March 2023

Published: 10 March 2023



Copyright: © 2023 by the authors. Licensee MDPI, Basel, Switzerland. This article is an open access article distributed under the terms and conditions of the Creative Commons Attribution (CC BY) license (<https://creativecommons.org/licenses/by/4.0/>).

Abstract: In this paper, a practical issue of the application of cubic boron nitride (CBN) cutting tools for the machining of steel 100Cr6 thin-walled bearing rings is addressed. Three geometries of the commercially available CBN cutting inserts were tested at different machining parameters. The effect of geometry was assessed in terms of surface integrity, considering 2D profile parameters, 3D topography of the surface, and residual stresses in the surface layer. The results were sometimes contradictory, since the same cutting inserts provided the largest and the lowest values of the topography parameters, dependent on different cutting conditions. In general, CBN cutting inserts with XCEL geometry ensured the smallest profile parameters R_a and R_z , and the spatial parameters of S_{mr1} exhibited the largest values among all tested tools, suggesting reduced wear resistance. Residual stresses analysis did not reveal any unacceptable or potentially dangerous surface layer state after machining.

Keywords: surface integrity; steel 100Cr6; CBN; cutting tool; cutting speed; cutting feed; cutting depth; bearing rings

1. Introduction

In smart manufacturing processes, the machine learning approach is widely used for the prediction of the effect of processing parameters on the final product [1]. In this context, it is inevitable to collect the maximal possible data on each machining process. Our case study is aimed at a practical application of the cutting tools of certain geometry, which is potentially feasible for intelligent tool selection with a predictable effect on the machined surface quality.

Composites based on cubic boron nitride (CBN) are commonly used for the fabrication of cutting tools destined for the fine finishing of functional surfaces due to their outstanding mechanical properties competing with diamonds [2]. CBN tools exhibit better chemical and thermal stability than diamond tools, and they are used to machine iron with high

hardness and heat-resistant alloys to fabricate various components such as shafts, bearings, gears, engine blocks, etc., with high dimensional accuracy and surface parameters using high cutting speed [3]. The wear resistance and durability of other cutting tool materials can reach only 50%, and after certain modifications it can be improved, but still reach no more than 75% of CBN tools wear resistance [4]. There are extensive studies published on the morphology of the CBN structure and its effect on cutting tool wear resistance [5–7]. Other studies analyzed the effect of various additions and binders in CBN composites [8]. Since some materials, such as compacted graphite iron, cause extensive wear of CBN tools, Zhu et al. published the results of their investigations on CBN tool wear with different metalworking fluids [9]. In an assessment of the tool life, surface integrity was found useful both in terms of the machined surface [10] and the surface of the cutting insert [11]. It is widely known that the performance of a machined component, including features such as fatigue strength, wear resistance, and tribological behavior, is closely correlated with the surface integrity obtained by machining. In general, the integrity of a machined surface is described as the relation of its mechanical, chemical, metallurgical, and topographical state to its functional characteristics [12]. A study on the cutting tool load effect on the machined surface aimed to statistically evaluate the real dynamic loads in correlation with surface roughness after milling [13]. Varga and his team analyzed the effect of a chosen milling strategy on the surface quality after the pocket milling process [14]. Willert et al. demonstrated that the ultrasonic assisted cutting process, compared with conventional machining, had the potential to improve the quality of a surface machined with CBN tools [15].

Specifically, Thiele and Melkote [16] investigated the influence of tool cutting edge geometry on the surface roughness in the finish hard turning of AISI 52100 steel. They found that the two-factor interaction between the workpiece hardness and cutting edge geometry had a substantial effect on the obtained surface roughness. It was also reported that after machining with large edge hone tools, deeper, more compressive residual stresses appeared in comparison with the ones after hone tools with small edges or chamfered tools [17]. Moreover, when harder materials underwent machining with chamfered tools, an increase in both the axial and the circumferential residual stresses has been reported for increased cutting speeds [18]. Adamik et al. examined the process of different geometry cutting edge wear and its effect on machined surface quality [19]. They pointed out that the flank wear had a large impact on the final component's quality in terms of surface integrity and roughness. Guddat and co-authors [20] suggested that some machining parameters, such as cutting speed, among others, had small effects on the surface quality and can be omitted in investigations. In contrast, the insert type and geometry had significant effects on surface roughness and residual stress. Even though no FEM-based methods have been proposed so far to predict the residual stresses after machining with wiper inserts, the authors reported that wiper inserts produced smoother surfaces and appeared to be more stable. Moreover, in their experiments, the application of wiper inserts provided better surface quality than conventional inserts.

In this context, practical application of the specific CBN cutting inserts in certain purpose-oriented conditions still requires additional investigation. This study is focused on the issue of CBN cutting insert geometry and its influence on the surface integrity of the machined surface, since there is no comprehensive study covering the problem and giving some practical recommendations. For instance, Zębala et al. analyzed the influence of cutting parameters on cutting forces and tool wear during the turning of Ni–Co alloy with CBN tools, also considering the topography and roughness parameters of the machined surface [21]. Latosińska et al. proposed a procedure for the optimization of finishing cutting parameters with minimized specific cutting force, also considering the quality of the machined surface [22]. Ociepa et al. studied the effects of coated and uncoated polycrystalline cubic boron nitride (PCBN) tools with TiN and TiAlN on the geometric parameters of the machined surface of hardened and tempered EN X153CrMoV12 steel [23]. Nikai et al. conducted a comprehensive study on the performance of different CBN inserts

with the same geometry but different coating technologies during the hard turning of AISI 4320 case-carburized steel [24].

In light of the available publications, it was decided to undertake the study involving different geometries of CBN cutting tools and surface integrity parameters of the machined thin-walled bearing rings, as follows. The issue is very important from the application perspective, since the selection of cutting tools includes edge geometry type, insert size, and insert grade [25] so that proper surface quality can be obtained.

2. Materials and Methods

The entire production process included a large number of variables that could affect the final product. In this study, attention was paid to the selected parameters, such as cutting tool geometry, cutting speed v_c , feed, and cutting depth a_p , which have a great influence on the evaluation of thin-walled bearing rings.

The experiments covered three groups of samples machined with respective cutting tools of different geometry denoted WIPEP, STANDARD, and XCEL. The cutting tool cubic boron nitride (CBN) inserts produced by Sandvik (Stockholm, Sweden) were used as follows:

- WIPER: insert CNGA120408T01030AWH class 7015 with WIPER geometry;
- STANDARD: insert CNGA120408S01030A with corner radius 0.8 mm;
- XCEL: insert CNGX1204L025-18AXA class 7015 with XCEL geometry.

The XCEL geometry has a straight edge with a small cutting-edge angle. This geometry helps to form thin chips, and the temperature at the cut point is reduced, slowing down of the development of wear in the form of a groove. Figures 1 and 2 present the inserts WIPER and XCEL, as well as the holder used in the experiments. It is clearly seen why no radius is given for the XCEL geometry. Figure 2b explains the geometrical difference between STANDARD and WIPER. The latter has multi-radii tool nose shaping designed for finish machining, where an additional flat section gives a smoother surface to the machined surface at a feed rate that is higher than usual [26].

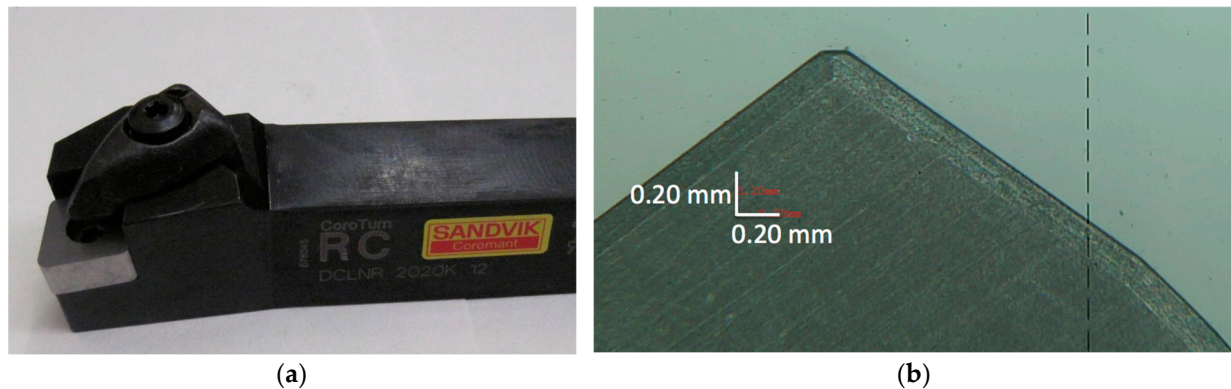


Figure 1. Experimental setup: (a) the holder with cutting insert; (b) insert CNGX1204L025-18AXA class 7015 with XCEL geometry.

The samples of bearing rings were made out of steel 100Cr6 (14 109.4) after thermal treatment as follows: normalizing annealing at 860 °C; soft annealing at 70 °C; cementation at 840 to 870 °C; quenching at 780 to 880 °C (oil to water); and tempering at 160 °C for 1 h. The declared properties were: strength R_m min. 785 MPa, R_e min. 590 MPa, and hardness min. 239 HB. The cutting operation was performed with a 3-axes machine tool Famar SUB160 (Famar, Avigliana, Italy). Since the producers recommended different machining parameters for each type of the cutting edge, it was decided to not repeat experiments in the same conditions for all tools, but to choose the most suitable settings for the respective geometries. Table 1 shows the experimental cutting parameters classified according to the group of samples.

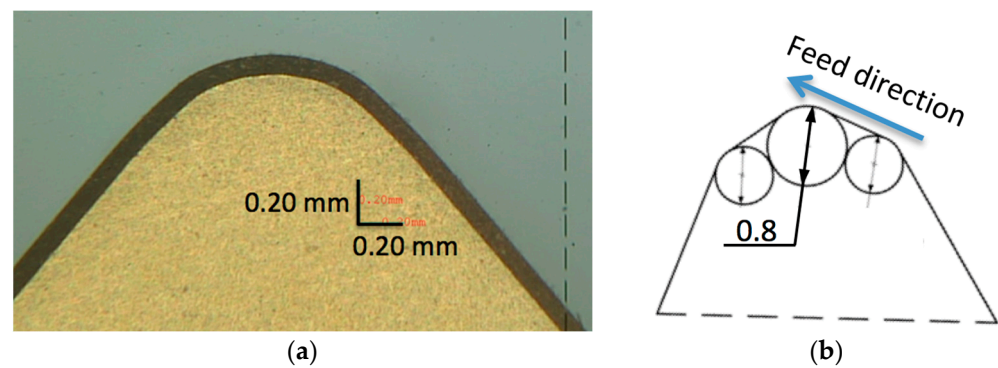


Figure 2. Insert CNGA120408T01030AWH class 7015 with WIPER geometry: (a) photo from microscope; (b) explanation of WIPER geometry.

Table 1. Machining parameters used in the experiments for the respective samples.

Sample Notion	Cutting Tool	Cutting Speed v_c (m/min)	Feed f (mm)	Cutting Depth a_p (mm)
O1	WIPER	180	0.28	0.3
O2		180	0.35	0.3
P1		195	0.28	0.1
P2		195	0.35	0.1
Q1	STANDARD	180	0.15	0.2
Q2		180	0.20	0.2
R1		195	0.15	0.4
R2		195	0.20	0.4
S1	XCEL	195	0.25	0.25
S2		195	0.35	0.25

The surface integrity of the machined bearings was assessed through the measurement of 2D roughness, 3D topography, and residual stresses of the outer layer. A large variety of surface measuring devices are available, from mechanical stylus profilometers and non-contact optical ones, to the scanning probe microscopes to be selected from in order to acquire either a cross-sectional profile or the areal topography information of the examined surfaces [27]. Some of the most recent reports cover investigations on optical measurement [28], especially diffractive relief structures [29] and interference microscopy [30] with confocal and spiral scanning [31], including comparative studies of different techniques [32]. Some researchers also discuss the comparability of different surface parameters obtained from profile and areal measurements [33,34].

In the present study, profile and topography parameters were measured using a 3D optical microscope Alicona InfiniteFocus G5 (Alicona, Graz, Austria). Its maximal measured area was 40,000 mm² at 2.5× zoom and 990 mm² at 100× zoom. For profile parameters, minimal mean arithmetic deviation of the profile at maximal zoom can be measured $Ra = 0.03 \mu\text{m}$, while for the topography measurement, the respective minimal measured value mean arithmetic height of the limited scale of the surface was $Sa = 0.015 \mu\text{m}$.

All profile parameters were measured under the conditions specified in ISO standards. When evaluating the surface with a roughness of RSm between 0.13 mm and 0.40 mm, the filter $\lambda_c = 0.8 \text{ mm}$ was used and the evaluation length was set to $l = 4 \text{ mm}$ according to the ČSN EN ISO 4288:1999 standard. The measurement was performed in a direction perpendicular to the measured part of the bearing ring, as shown in Figure 3a. On the entire circumference of the bearing ring, three areas with the dimensions of 4 mm × 4 mm were measured in the range of 120°. On each scanned area, 5 paths were measured, as shown in Figure 3b, where the straight lines were evenly distributed over the surface of scanned area.

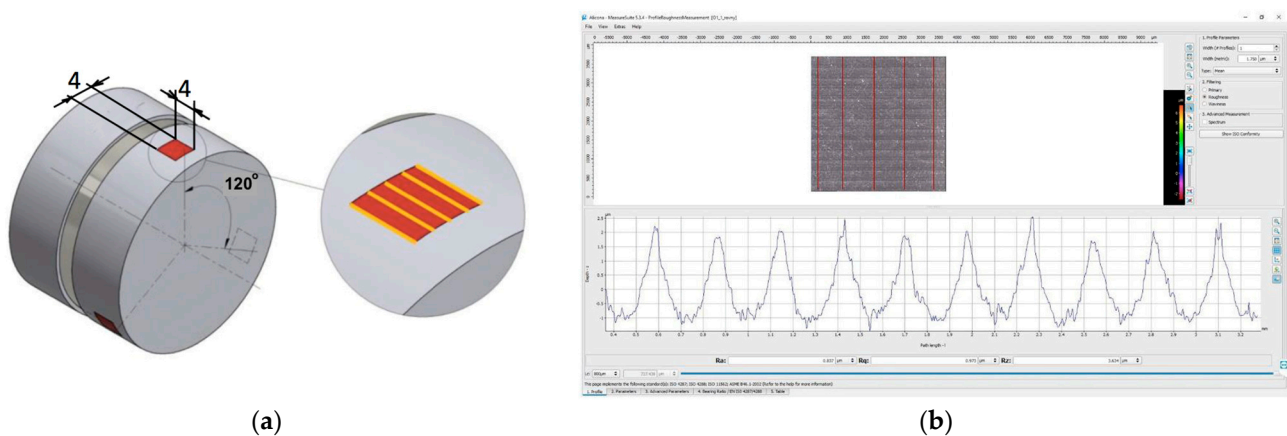


Figure 3. Measurement of the profile parameters: (a) scanned area on the bearing surface; (b) example of the screen during profile measurement, where red lines correspond with analyzed profiles on the scanned area.

Among the profile parameters, R_a (mean arithmetic deviation of the profile), R_z (the largest height of the profile), and $Rmr(c)$ (material proportion of the profile) were considered. R_a is the most frequently used roughness parameter, but it is not sensitive to the height fluctuations of the evaluated surface profile. Therefore, the R_z parameter was also monitored, especially as it was required by the bearing technical documentation. Additionally, $Rmr1$ was required by the documents to be checked. $Rmr1$ is the material proportion of the profile (supporting proportion), defined as the material ratio of the protrusions (vertices) to the core of the material surface. The material proportion of the profile is typical for individual finishing methods, and its value is especially important for the assessment of loaded functional surfaces, such as friction, lubrication, and wear.

Traditionally, the evaluation of surface quality using profile (2D) parameters is common in engineering practice, but nowadays, 3D surface analysis is available and can provide crucial information on surface integrity. To perform the area measurement of the surface texture, three measured areas $4\text{ mm} \times 4\text{ mm}$ were scanned and distanced by 120° , as shown in Figure 4. From the measured areas with dimensions of $2\text{ mm} \times 2\text{ mm}$, the height parameters of the surface texture were selected according to the standard ČSN EN ISO 25 178–2. Following the standard ČSN EN ISO 25 178–3, a Gaussian filter of 0.8 mm was used for the calculation of spatial parameters.

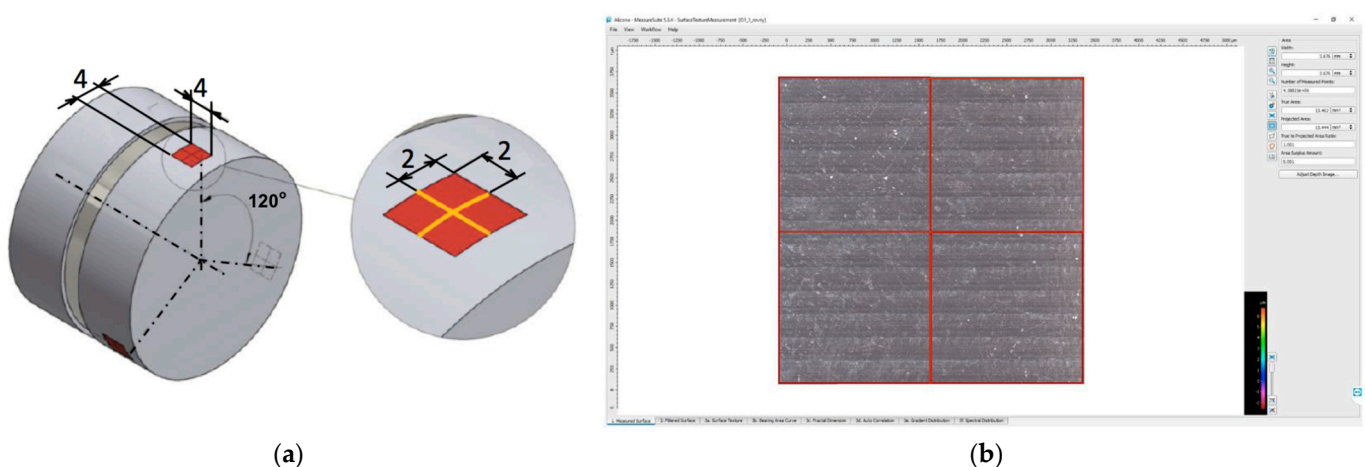


Figure 4. Measurement of the surface topography parameters: (a) scanned area on the bearing surface; (b) example of the screen during measurement, where red lines divide the scanned area into four analyzed sections.

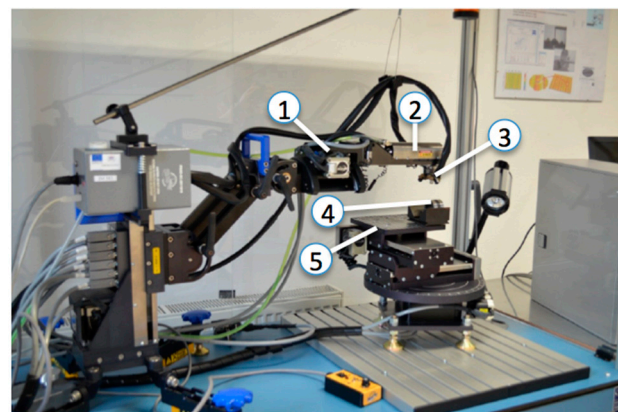
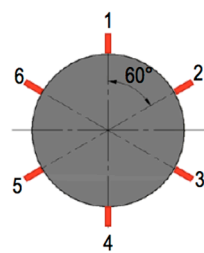
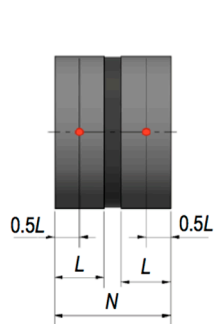
In the analysis, the following parameters were considered: Sa (mean arithmetic height of the limited scale of the surface), Sz (maximum height of the limited scale of the surface), and $Smr1$ (material proportion of the surface), which somehow corresponded with the 2D parameters listed above.

The parameter Sa is the most frequently used one; it represents spatial characteristics that correspond to the roughness profile parameter Ra . However, it is far more accurate and able to capture the maximum peak height and maximum depth from the entire scanned surface. The bearing surface parameters represented by Sa are also important for functional properties, such as resistance during start-up and run-down of the bearing, low coefficient of friction, and friction contact with the bearing pin.

Another analyzed surface parameter was Sz , basically representing the sum of the highest peaks and the deepest depressions found on the measured surface. The Sz parameter is suitable for assessing the service life of the component, the sealing ability of the surfaces, etc. In the case of bearing, unevenness on the surface is particularly dangerous, as it may result in cracks, with further development of stress concentrators and the occurrence of fatigue damage. Therefore, it is important to monitor the surface integrity through statically stable surface topography parameter Sz .

The last analyzed surface parameter was the $Smr1$, which represented the material fraction of the surface (carrying fraction). It is sensitive to the material surface protrusion, which may pose problems during the interfacial contact of the surfaces, causing microdamage.

The residual stress measurements were performed using a Proto iXRD device (Proto Manufacturing Ltd., Oldcastle, ON, Canada) on the outer circumference of the bearing rings in the axial half of the surface and at six angular positions. Due to the principle of diffraction, it was necessary to ensure that the surface of the analyzed samples did not contain any dirt or grease, avoiding mechanical treatment in order to minimize any influence that may negatively affect the measurement result. It is recommended to apply chemical cleaning. After proper positioning of the sample, the measurement was performed through Proto XrdWin operating software. After starting the measurement, the diffracted beam was recorded on the detectors, then digitized via an A/D converter and evaluated by the XrdWin program. Measurement positions are shown in Figure 5 together with the device Proto iXRD, and the example of the screen with the results is presented in Figure 6.



(a)

(b)

Figure 5. Measurement of the residual stress: (a) positions of the measuring points; (b) diffractometer Proto iXRD: 1—measuring arm, 2—X-ray lamp, 3—two detectors capturing the diffraction cone, 4—examined sample, 5—adjustable and rotating table.

The settings of the X-ray diffractometer during the measurement were based on the material characteristics of the ring and the heat treatment of the material, where the predominant martensitic structure was assumed.

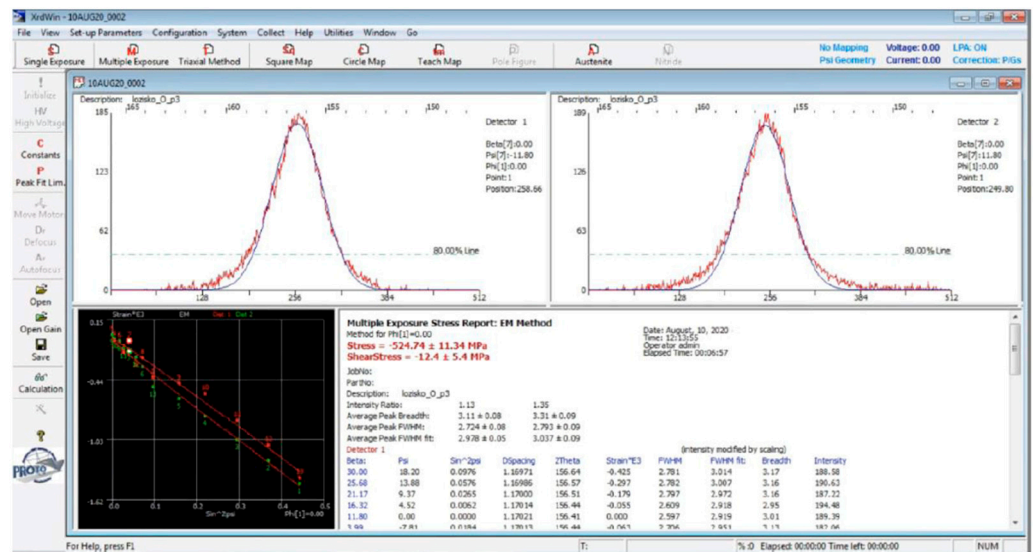


Figure 6. Example of a screen with the results of residual stress measurement.

3. Results and Discussion

The surface integrity of the bearing rings was analyzed in terms of geometrical features of the surface and residual stresses in the upper layer. Surface geometry measurements were divided into 2D (profile) and 3D (topography) analysis, while normal residual stresses were distinguished from shear stresses.

3.1. Profile and Topography Measurement Results

Figure 7 presents a comparison of the profile parameters Ra obtained for different samples. Since the measurement was repeated for each sample, the average results are shown. In the diagram, 3D parameter Sa is presented, too. In general, there was no significant difference between 2D and 3D results, because the Sa parameter does not distinguish between peaks and valleys. In most of the bearing rings, the dispersion of the results was quite similar. A significant difference was seen in bearing ring O1, where 3D parameter Sa exhibited the largest dispersion of ca. $0.2 \mu\text{m}$. This difference was due to the measurement of a larger area where some unevenness was noted, unnoticed by the profile measurement. These local deviations could have appeared either through mishandling of the sample or a manufacturing error.

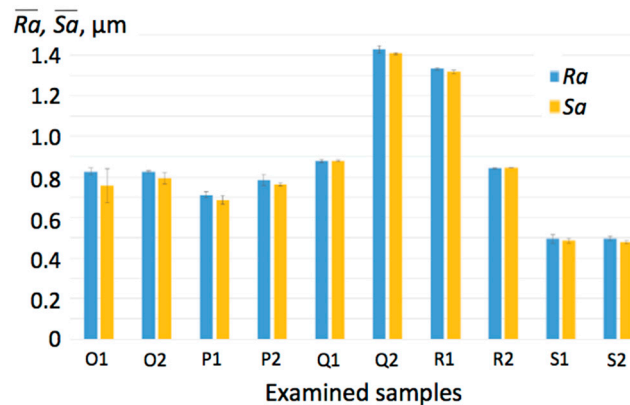


Figure 7. Average results of profile roughness \overline{Ra} and respective 3D parameter \overline{Sa} measurement of the examined samples.

From the graph in Figure 7, it can be noted that the largest value Ra appeared in the rings Q2 ($Ra = 1.429 \mu\text{m}$) and R1 ($Ra = 1.333 \mu\text{m}$). Both samples were machined with

the cutting tool denoted STANDARD. In contrast, the smallest measured Ra values were obtained for rings S1 ($Ra = 0.494 \mu\text{m}$) and S2 ($Ra = 0.496 \mu\text{m}$). These samples were machined with the XCEL tool. In these cases, STANDARD cutting inserts produced surfaces with three times higher roughness Ra than those machined by XCEL inserts.

The results of roughness measurement Rz and respective topography Sz are shown in Figure 8. The overall trend of Rz is similar to the one exhibited by Ra ; namely, the highest values were obtained for Q2 and R1 samples, while the lowest were obtained for S1 and S2 ($Rz = 2.375$ and $2.308 \mu\text{m}$, respectively). Hence, the XCEL geometry of CBN cutting inserts contributed to the best roughness of the machined surface. However, even these lowest values did not fit the tolerance specified in the technical documentation, $Rz = 1.6 \mu\text{m}$. This result can be evaluated as indicating a poor state of surface integrity, which is unfavorable for the functionality of the component and its durability.

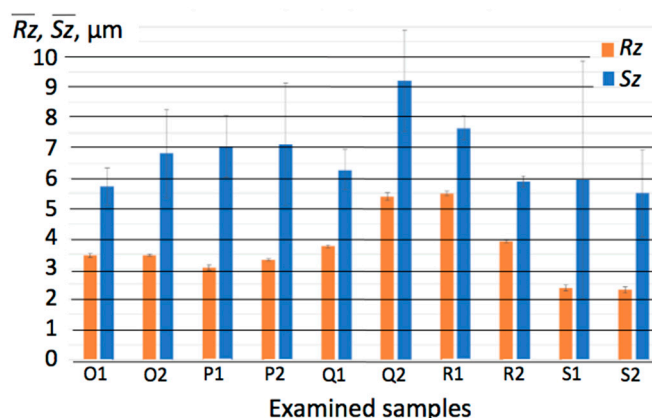


Figure 8. Average results of profile height \overline{Rz} and respective topography height \overline{Sz} measurement of the samples.

From the graph in Figure 8, it is seen that the largest values for the surface parameter Sz were obtained for bearing rings Q2 ($Sz = 9.217 \mu\text{m}$) and R1 ($Sz = 7.657 \mu\text{m}$) machined with the STANDARD tool. Considering the especially large dispersion of the results $\pm 2 \mu\text{m}$ for the Q2 sample, greater wear of this component can be expected. On the other hand, the smallest surface parameters Sz were measured for bearing rings S2 ($Sz = 5.499 \mu\text{m}$) and S1 ($Sz = 5.499 \mu\text{m}$) machined with the XCEL tool, but also for O1 ($Sz = 5.731 \mu\text{m}$) machined with the WIPER tool and R2 ($Sz = 5.885$) for the STANDARD tool. Considering the requirements related to the thin-walled bearing rings, it can be assumed that the surface integrity of these four samples significantly reduced the risk of a crack forming, and thus increased the service life of the bearing. Notably, two out of four of the samples that exhibited a low Sz parameter were fabricated using the cutting inserts of XCEL geometry.

It should be noted, however, that the Sz results for both samples S1 and S2 showed very high dispersion. Specifically, the S1 ring exhibited a dispersion of $\pm 4 \mu\text{m}$, which indicated low repeatability of the appearance of the highest peaks and the deepest depressions throughout the surface of the ring.

A representation of the material proportion of the profile $Rmr1$ and surface $Smr1$ is presented in the diagram in Figure 9.

Some different trends can be seen than those for the previous parameters Ra and Rz . The smallest profile peak material fractions were observed in S2 rings (21.365%) machined with the XCEL tool, and P1 rings (22.497%) machined with the WIPER tool. These rings may be expected to have a longer service life compared with the others due to the least number of peaks causing slower wear. Additionally, this feature has a beneficial effect on the functionality of the part. However, the disadvantage is that it can have less tightness due to a larger ratio of the surface core and greater contact stress. Interestingly, both the WIPER and XCEL tools produced the largest $Rmr1$ values. The largest material share had ring Q2 ($Rmr1 = 32.269\%$) made with the STANDARD tool, but also the S1 sample ($Rmr1 =$

31.303%) fabricated with the XCEL tool and the O2 sample ($Rmr1 = 31.214\%$) machined with the WIPER tool. These rings can be expected to have the greatest tightness but the worst lubricating ability. In all cases of measured rings, there was a greater variance concerning the Ra and Rz parameters, which may be a result of cutting tool traces on the surface. The acceptable rate according to the drawings was $Rmr1 \geq 10\%$ and this requirement was fulfilled by all the examined cutting tools.

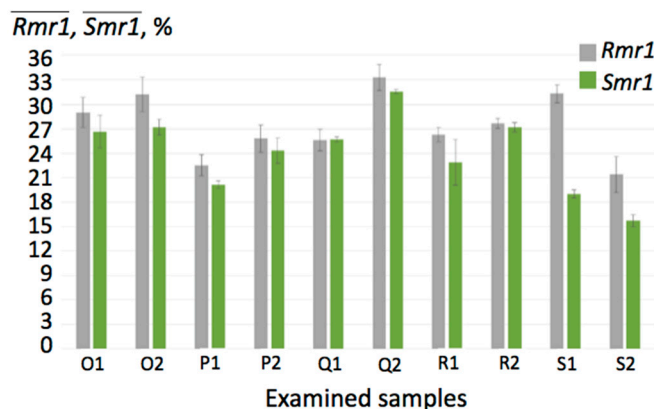


Figure 9. Average results on a material proportion of the profile $\overline{Rmr1}$ and respective topography parameter $\overline{Smr1}$ of the bearing ring samples.

The largest values of spatial parameter $Smr1$ found in Figure 9 were for thin-walled bearing rings Q2 (31.543%) and O2 (27.149%) machined with the WIPER tool, and for the R2 sample (27.156%) machined with the STANDARD tool. This parameter indicated that WIPER geometry of the CBN tool might have contributed to the slower wear of the surface, longer service life, and better functionality of the bearing ring. In this case, the smallest measured parameters $Smr1$ were obtained for the samples S2 (15.684%) and S1 (18.985%), both machined with the XCEL tool. This may result in a shortened life of the bearing rings due to the rapid wear of the sliding surface.

As would be expected, there is no single profile or surface parameter that unequivocally ensures a long service time of the bearing ring, and there is no single cutting tool that may be considered ‘the best’ one. Therefore, apart from geometrical surface features, residual stresses in the upper layer should be taken into consideration.

3.2. Residual Stresses

In general, compressive stresses are considered beneficial to the fatigue life of the machined part, its creep life, and resistance to cracking under stress corrosion, while tensile residual stresses are rather harmful [35]. Residual stresses σ on rings were compressive in all analyzed positions, i.e., all their values were negative. From the practical perspective of an inner surface of bearing, this nature of the stresses can be considered favorable in terms of the component functionality and surface integrity. Figure 10a shows the diagram of normal residual stresses for samples O1 and O2 machined with the WIPER tool. On the surface of O2, it is seen that the differences between the values obtained in the areas around the cylinder were less dispersed compared with O1. In the case of O2 samples, the difference between the lowest and the highest value was found to be only around 50 MPa, which is about 10%, while O1 samples exhibited dispersion of the results of ca. 125 MPa, which is close to 20%. In turn, comparison between P1 and P2 samples (Figure 10b) showed that residual stresses varied from 450 MPa up to 540 MPa in P1, while P2 exhibited dispersion varied from 500 MPa up to 690 MPa. The samples P1 and P2 were machined with the same WIPER tool, but at higher cutting speed.

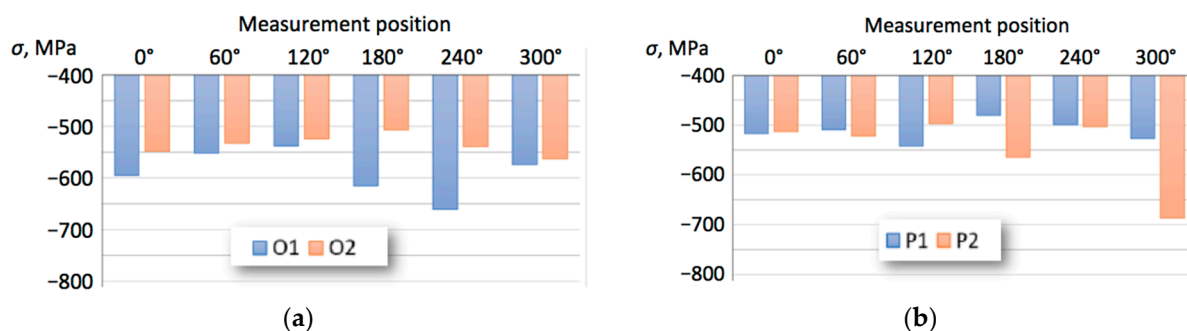


Figure 10. Comparison of normal residual stresses σ after machining with WIPER insert: (a) samples O1 and O2; (b) samples P1 and P2.

Other machining methods generated much higher residual stresses in the upper layer of material, as presented in Figure 11. The lowest absolute value of stress σ obtained for the Q1 sample was 630 MPa, which was close to the highest values for the respective O1 and O2 samples. The rest of the tested samples exhibited higher absolute values of residual stress.

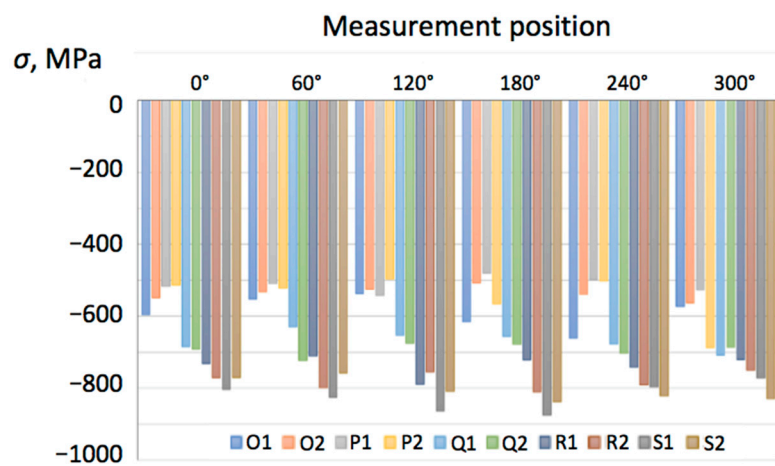


Figure 11. Results of normal residual stress σ measurement.

Based on the graph in Figure 11, it can be concluded that all examined replaceable cutting inserts have generated a certain strengthening of the surface layer, which was manifested by the formation of compressive normal residual stresses. Thus, it is possible to assume a sufficient service life of the machined part. It should be noted that the highest compressive normal residual stresses were identified in the surface layers machined with XCEL cutting inserts denoted as S1 and S2. Variations between individual measurements in different angular positions were found to be close to 100 MPa, which was approximately 12–15%.

Notably, it was suggested in the literature [20] that the wiper geometry of the tool enlarged the contact area between the cutting edge and the workpiece, which resulted in higher compressive residual stress. In our study, it appeared that the WIPER cutting inserts denoted O and P generated all the smallest absolute values of stress σ below 600 MPa.

In addition to normal residual stresses, shear stresses τ were also identified in the surface layer of the bearing rings. Their values are presented in the diagram shown in Figure 12. The presence of shear stress represents the displacement of individual microstructural layers of the material, resulting from imperfect cutting or excessive stretching of the material during the machining process.

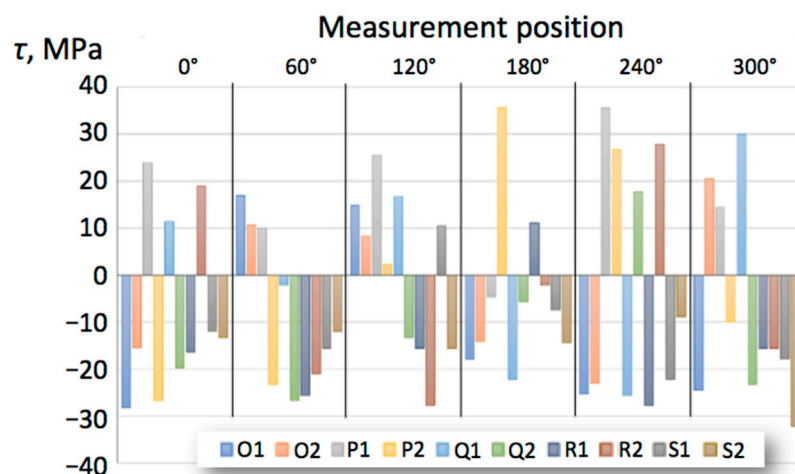


Figure 12. Results of shear stress τ measurement.

In general, shear stresses τ were both negative and positive, but their absolute values did not exceed 40 MPa. Due to their low values compared with the material yield strength $R_e = 590$ MPa, the shear stresses can be considered negligible from the perspective of functionality and wear resistance. This observation leads to the conclusion that none of the tested cutting inserts generated outstanding shear stresses inside the surface layer of the machined bearing ring.

Residual stresses appear due to the friction forces between the cutting tool insert and the workpiece surface, with thermal and mechanical loads resulting in the distribution of stress along the material. Inhomogeneous plastic deformation induced by mechanical and thermal loads is associated with the chip formation process. Moreover, the squeezing interaction between the freshly machined material and tool nose region contributes to the formation of the residual stresses. Among variable parameters affecting the residual stresses, the tool quality appears to be the most influential one [35]. Apart from the main geometry, which was to be chosen in this study for determining further application, other geometrical features should be investigated in the future, such as the rounding corresponding to the transition between the rake face and the flank face. It can be different for different insert geometries, and, despite the high repeatability of cutting inserts, it may differ from one piece to other. Due to ploughing effects, it may have an effect on the development of residual stresses.

4. Concluding Remarks

The cutting tool inserts made out of cubic boron nitride (CBN) with different geometries were examined in terms of the resulting surface integrity of the machined surface of a thin-walled bearing ring. Three insert types were used in the experiments: CNGA120408T01030AWH class 7015 with WIPER geometry, STANDARD insert CNGA120408S01030A with corner radius $R_E = 0.8$ mm, and insert CNGX1204L025-18AXA class 7015 with XCEL geometry. In terms of surface integrity, some obtained results can indicate the feasibility of the selected cutting tools for this particular task, as follows.

The smallest profile roughness parameters R_a and R_z values were obtained for the samples machined with XCEL cutting tools. However, none of the examined inserts and applied machining parameters ensured the fulfillment of the prescribed tolerance condition of $R_z = 1.6$ μm . From the results of the R_{mr1} , a different trend can be seen. The rings P1 and S2 (WIPER and XCEL) had the smallest material share of the peak, while the rings Q2 and S1 (again, WIPER and XCEL, but with different cutting conditions) had the largest material share. All tested inserts ensured an acceptable limit rate according to the document, $R_{mr1} \geq 10\%$.

On the other hand, among 3D parameters, the largest S_a values were obtained for bearing rings machined with STANDARD tools, while the smallest S_a were obtained

with XCEL tools. Similarly, STANDARD tool inserts provided the largest values for the parameter S_z , and the smallest values of S_z were again obtained with STANDARD tools, but at different cutting conditions. Moreover, the smallest S_z values were those obtained with XCEL inserts. Notably, WIPER inserts provided the largest dispersion of the spatial topography parameters. In turn, the largest values of S_{mr1} appeared for thin-walled bearing rings machined with WIPER and STANDARD cutting tools, which suggested lower service life and rapid wear of the rings machined with XCEL tools.

Another component of the surface integrity, residual stress in the upper layer, indicated that all examined inserts provided a certain surface hardening of the rings. Hence, it is possible to assume a sufficient service life of the part. The highest compressive normal residual stresses were identified in the surfaces layers of the rings machined with XCEL cutting tools. The stress value variations in the individual rings were around 10%, while their absolute values ranged from 500 to 850 MPa. Additionally, shear stresses were also identified since they corresponded with the displacement of individual microstructural layers inside the material, indicating an imperfect cutting process or excessive stretching of the material. In general, their absolute values did not exceed 40 MPa. Due to the low values compared with the yield strength $R_e = 590$ MPa, their effect on the functionality and durability of the bearing rings can be considered negligible.

Thus, it can be stated that STANDARD cutting inserts were able to ensure both the largest and the lowest S_a and S_z values, dependent on cutting conditions. The largest, rather favorable value of S_{mr1} was a result of work with STANDARD cutting tools, too.

The rings machined with WIPER tools had one of the smallest material shares of the peak $R_{mr1} = 23\%$, while at different cutting conditions the material share could reach $R_{mr1} = 31\%$. Large values of $S_{mr1} = 27\%$ were achieved after machining with WIPER.

XCEL cutting inserts ensured the smallest profile parameters R_a and R_z , but R_{mr1} appeared to be the smallest for the larger feed value $f = 0.35$ mm, while the reduced feed of 0.25 mm provided one of the highest values of $R_{mr1} = 31\%$. Similarly, spatial parameters S_a were the smallest for XCEL tools, but the values of S_{mr1} appeared to be the smallest.

At this stage of the investigation it can be stated that most of the parameters are favorable after XCEL machining. From the practical perspective, it should be further investigated if the small values of S_{mr1} reduce the service time of bearing rings made with XCEL inserts compared with other samples. Moreover, it is necessary to find out and eliminate the factors that caused too-high R_z after cutting with all types of inserts.

Author Contributions: Conceptualization, L.C. (Lenka Cepova), O.M. and M.R.; methodology, L.C. (Lenka Cepova), M.R. and R.C.; validation, R.C., M.T., L.B. and S.D.; formal analysis, M.T., M.R., V.C. and L.B.; investigation, L.C. (Lenka Cepova), L.C. (Leszek Chalko), and S.D.; data curation, M.T., O.M. and L.C. (Lenka Cepova); writing—original draft preparation, L.C. (Lenka Cepova), O.M. and L.C. (Leszek Chalko); writing—review and editing, R.C., M.R., V.C. and S.D.; visualization, V.C.; supervision, R.C., L.B. and S.D.; project administration, R.C. All authors have read and agreed to the published version of the manuscript.

Funding: This article has been completed in connection with the projects Education System for Personal Resource of Development and Research in the Field of Modern Trend of Surface Engineering—surface integrity, reg. no. CZ.1.07/2.3.00/20.0037 financed by the Structural Funds of the European Union, from the means of the state budget of the Czech Republic, by the projects Students Grant Competition SP2022/50 and SP2022/131 financed by the Ministry of Education, Youth and Sports, and the Faculty of Mechanical Engineering VŠB-TUO.

Institutional Review Board Statement: Not applicable.

Informed Consent Statement: Not applicable.

Data Availability Statement: Data are available on request.

Acknowledgments: The authors express their gratitude to the company KOYO BEARINGS and colleagues from the Engineering Faculty, University of Zilina, Czech Republic, for their technical support. The authors are thankful especially to Dagmar Mikulová for her contribution to the investigations.

Conflicts of Interest: The authors declare no conflict of interest.

Nomenclature

Roughness/Surface Topography Parameters

l	evaluation length, mm;
Ra	mean arithmetic deviation of the profile, μm ;
$Rmr(c)$	material proportion of the profile, μm ;
$Rmr1$	material proportion of the profile (supporting proportion), defined as the material ratio of the protrusions (vertices) to the core of the material surface, %;
Rz	the largest height of the profile, μm ;
Sa	mean arithmetic height of the limited scale of the surface, μm ;
$Smr1$	material proportion of the surface, %;
Sz	the maximum height of the limited scale of the surface, μm ;
λ_c	cut-off filter, mm.

Machining Process Parameters

a_p	cutting depth, mm;
f	feed, mm;
v_c	cutting speed, m/min.

Material Properties

R_e	yield strength, MPa;
R_m	tensile strength, MPa;
σ	normal residual stress;
τ	shear stress.

References

- Yu, J.; Oh, S.J.; Baek, S.; Kim, J.; Lee, T. Predicting the Effect of Processing Parameters on Caliber-Rolled Mg Alloys through Machine Learning. *Appl. Sci.* **2022**, *12*, 10646. [\[CrossRef\]](#)
- Monteiro, S.N.; Skury, A.L.D.; de Azevedo, M.G.; Bobrovnitchii, G.S. Cubic boron nitride competing with diamond as a superhard engineering material—An overview. *J. Mater. Res. Technol.* **2013**, *2*, 68–74. [\[CrossRef\]](#)
- Jain, A.; Bajpai, V. Introduction to high-speed machining (HSM). In *High Speed Machining*; Gupta, K., Davim, J.P., Eds.; Academic Press: London, UK, 2020; pp. 1–25. [\[CrossRef\]](#)
- Gevorkyan, E.; Rucki, M.; Sałaciński, T.; Siemiątkowski, Z.; Nerubatskyi, V.; Kucharczyk, W.; Chrzanowski, J.; Gutsalenko, Y.; Nejman, M. Feasibility of Cobalt-Free Nanostructured WC Cutting Inserts for Machining of a TiC/Fe Composite. *Materials* **2021**, *14*, 3432. [\[CrossRef\]](#) [\[PubMed\]](#)
- Fang, S. Morphological study of a cubic boron nitride (CBN) cutting tool and characterization of its wear scenarios in abrasive machining process. *Ceram. Int.* **2020**, *46 Pt B*, 19491–19498. [\[CrossRef\]](#)
- Wang, J.; Yu, T.; Ding, W.; Fu, Y.; Bastawros, A.F. Wear evolution and stress distribution of single CBN superabrasive grain in high-speed grinding. *Precis. Eng.* **2018**, *54*, 70–80. [\[CrossRef\]](#)
- Binder, M.; Klocke, F.; Doeblener, B. Abrasive wear behavior under metal cutting conditions. *Wear* **2017**, *376–377 Pt A*, 165–171. [\[CrossRef\]](#)
- Liu, Y.; Zhang, W.; Peng, Y.; Fan, G.; Liu, B. Effects of TiAl Alloy as a Binder on Cubic Boron Nitride Composites. *Materials* **2021**, *14*, 6335. [\[CrossRef\]](#)
- Zhu, L.; Evans, R.; Zhou, Y.; Ren, F. Wear Study of Cubic Boron Nitride (cBN) Cutting Tool for Machining of Compacted Graphite Iron (CGI) with Different Metalworking Fluids. *Lubricants* **2022**, *10*, 51. [\[CrossRef\]](#)
- Iqbal, A.; Zhao, G.; Cheok, Q.; He, N.; Nauman, M.M. Sustainable Machining: Tool Life Criterion Based on Work Surface Quality. *Processes* **2022**, *10*, 1087. [\[CrossRef\]](#)
- Narojczyk, J.; Morozow, D.; Narojczyk, J.W.; Rucki, M. Ion implantation of the tool's rake face for machining of the Ti-6Al-4V alloy. *J. Manuf. Process.* **2018**, *34 Pt A*, 274–280. [\[CrossRef\]](#)
- Li, J.; Tian, Y.; Fang, Q. Molecular dynamics simulation of friction, lubrication, and tool wear during nanometric machining. In *Machining and Tribology*; Pramanik, A., Ed.; Elsevier: Amsterdam, The Netherlands, 2022; pp. 187–211. [\[CrossRef\]](#)
- Frydrýšek, K.; Skoupý, O.; Mrkvička, I.; Slaninková, A.; Kratochvíl, J.; Jurga, T.; Vlk, M.; Krpec, P.; Madeja, R.; Havlíček, M.; et al. Stochastic Evaluation of Cutting Tool Load and Surface Quality during Milling of HPL. *Appl. Sci.* **2022**, *12*, 12523. [\[CrossRef\]](#)
- Varga, J.; Tóth, T.; Kašćák, L.; Spišák, E. The Effect of the Machining Strategy on the Surface Accuracy When Milling with a Ball End Cutting Tool of the Aluminum Alloy AlCu4Mg. *Appl. Sci.* **2022**, *12*, 10638. [\[CrossRef\]](#)

15. Willert, M.; Zielinski, T.; Rickens, K.; Riemer, O.; Karpuschewski, B. Impact of ultrasonic assisted cutting of steel on surface integrity. *Procedia CIRP* **2020**, *87*, 222–227. [[CrossRef](#)]
16. Thiele, J.D.; Melkote, S.N. Effect of cutting edge geometry and workpiece hardness on surface generation in the finish hard turning of AISI 52100 steel. *J. Mater. Process. Technol.* **1999**, *94*, 216–226. [[CrossRef](#)]
17. Thiele, J.D.; Melkote, S.N. Effect of Tool Edge Geometry on Workpiece Subsurface Deformation and Through-Thickness Residual Stresses for Hard Turning of AISI 52100 Steel. *J. Manuf. Process.* **2000**, *2*, 270–276. [[CrossRef](#)]
18. Caruso, S.; Umbrello, D.; Outeiro, J.C.; Filice, L.; Micari, F. An Experimental Investigation of Residual Stresses in Hard Machining of AISI 52100 Steel. *Procedia Eng.* **2011**, *19*, 67–72. [[CrossRef](#)]
19. Adamik, M.; Drlička, R.; Matúš, M.; Žitňanský, J. Effectiveness of Hard Turning. *Adv. Mater. Res.* **2013**, *801*, 109–116. [[CrossRef](#)]
20. Guddat, J.; M'Saoubi, R.; Alm, P.; Meyer, D. Hard turning of AISI 52100 using PCBN wiper geometry inserts and the resulting surface integrity. *Procedia Eng.* **2011**, *19*, 118–124. [[CrossRef](#)]
21. Zębala, W.; Struzikiewicz, G.; Rumian, K. Cutting Forces and Tool Wear Investigation during Turning of Sintered Nickel-Cobalt Alloy with CBN Tools. *Materials* **2021**, *14*, 1623. [[CrossRef](#)] [[PubMed](#)]
22. Latosińska, K.; Struzikiewicz, G.; Zębala, W. Method of Data Selection for Turning of Inconel 718 Alloy Obtained by Casting and Laser Sintering Powder. *Materials* **2022**, *15*, 1448. [[CrossRef](#)]
23. Ociepa, M.; Jenek, M.; Kuryło, P. The Geometric Surface Structure of EN X153CrMoV12 Tool Steel after Finish Turning Using PCBN Cutting Tools. *Coatings* **2021**, *11*, 428. [[CrossRef](#)]
24. Niaki, F.A.; Haines, E.; Dreussi, R.; Weyer, G. Machinability and Surface Integrity Characterization in Hard Turning of AISI 4320 Bearing Steel Using Different CBN Inserts. *Procedia Manuf.* **2020**, *48*, 598–605. [[CrossRef](#)]
25. Phung, X.L.; Truong, H.S.; Bui, N.T. Expert System Based on Integrated Fuzzy AHP for Automatic Cutting Tool Selection. *Appl. Sci.* **2019**, *9*, 4308. [[CrossRef](#)]
26. Correia, A.E.; Davim, J.P. Surface roughness measurement in turning carbon steel AISI 1045 using wiper inserts. *Measurement* **2011**, *44*, 1000–1005. [[CrossRef](#)]
27. Gao, W.; Haitjema, H.; Fang, F.Z.; Leach, R.K.; Cheung, C.F.; Savio, E.; Linares, J.M. On-machine and in-process surface metrology for precision manufacturing. *CIRP Ann.* **2019**, *68*, 843–866. [[CrossRef](#)]
28. Jiao, F.; Liu, L.; Cheng, W.; Li, C.; Zhang, X. Review of optical measurement techniques for measuring three-dimensional topography of inner-wall-shaped parts. *Measurement* **2022**, *202*, 111794. [[CrossRef](#)]
29. Lu, W.; Chen, S.; Zhang, K.; Zhai, D. Characterization of diffractive relief structures over large areas by stitching interference microscopic topography. *Measurement* **2022**, *202*, 111850. [[CrossRef](#)]
30. Guo, J.; Zhai, D.; Lu, W.; Chen, S. Topography measurement of helical grooves on a hemisphere based on stitching interference microscopy. *Opt. Laser Technol.* **2022**, *152*, 108133. [[CrossRef](#)]
31. Ying, R.; Cui, Y.; Huang, J.; Liang, D.; Wang, Y. Precise measurement of surface topography with microstructures based on differential confocal and spiral scanning. *Measurement* **2021**, *184*, 110004. [[CrossRef](#)]
32. Leksycki, K.; Królczyk, J.B. Comparative assessment of the surface topography for different optical profilometry techniques after dry turning of Ti6Al4V titanium alloy. *Measurement* **2021**, *169*, 108378. [[CrossRef](#)]
33. Schmidt, J.; Thorenz, B.; Schreiner, F.; Döpfer, F. Comparison of areal and profile surface measurement methods for evaluating surface properties of machined components. *Procedia CIRP* **2021**, *102*, 459–464. [[CrossRef](#)]
34. Svetlik, J.; Baron, P.; Dobransky, J.; Kocisko, M. Implementation of computer system for support of technological preparation of production for technologies of surface processing. In *Applied Mechanics and Materials, Proceedings of the ROBTEP 2014: 13th International Conference on Industrial, Service and Humanoid Robotics, High Tatras, Slovakia, 15–17 May 2014*; Trans Tech Publications Ltd.: Zurich, Switzerland, 2014; Volume 613, pp. 418–425. ISBN 978-303835202-0. [[CrossRef](#)]
35. Oliveira, A.R.F.; da Silva, L.R.R.; Baldin, V.; Fonseca, M.P.C.; Silva, R.B.; Machado, A.R. Effect of tool wear on the surface integrity of Inconel 718 in face milling with cemented carbide tools. *Wear* **2021**, *476*, 203752. [[CrossRef](#)]

Disclaimer/Publisher's Note: The statements, opinions and data contained in all publications are solely those of the individual author(s) and contributor(s) and not of MDPI and/or the editor(s). MDPI and/or the editor(s) disclaim responsibility for any injury to people or property resulting from any ideas, methods, instructions or products referred to in the content.